Received: November 4, 2023. Revised: December 17, 2023. 880

International Journal of
Intelligent Engineering & Systems

http://www.inass.org/

Channel Fusion Filter and Invariant Scattering Network-Based Leukocyte Image Discrimination Framework

Renuka Veerappa Tali[1]* **Surekha Borra[2]**

[1]*Department of ECE, K. S. School of Engineering and Management, VTU, Bengaluru, Karnataka, India*
[2]*Department of Computer Science and Engineering (IoT & Cyber Security Including Blockchain Technology), K. S. Institute of Technology, VTU, Bengaluru, Karnataka, India*
* Corresponding author's Email: renukavtali@gmail.com

Abstract: The escalating demand for accessible, effective, and precise healthcare solutions has driven extensive research into integrating artificial intelligence into the medical field. Recognizing intricate patterns within biomedical images remains a formidable challenge for human practitioners. In response to this, our study introduces a pioneering image enhancement paradigm, the stationary wavelet channel fusion filtered (SWCFF) algorithm. Additionally, we employ the invariant scattering network (ISN), a novel feature learning methodology to analyze leukocyte images. The novelty of our approach lies in the inventive combination of SWCFF and ISN for enhanced feature extraction and discrimination of leukocytes. Our investigation aims to assess the efficacy of automatically extracted features from this algorithm in differentiating leukocytes, leveraging a support vector machine (SVM) classifier for the diagnosis and detection of leukemia and other blood-related conditions. The proposed model is rigorously evaluated on four benchmark datasets: ALLIDB, C_NMC, BCCD, and LISC. Notably, the ALLIDB binary class achieves a peak accuracy of 96.15% (95% CI: 0.9 to 1), while the class accuracy for neutrophils reaches an impressive 97.96% (95% CI: 0.89 to 1), accompanied by a precision of 100% and a false positive rate of 0%. Our innovative approach holds promise for the deployment of a cost-effective computer-aided diagnosis (CAD) tool in rural settings, aiding physicians in early disease prediction and the timely monitoring of treatment.

Keywords: Acute lymphoblastic leukemia, Image fusion, Leukocyte, Machine learning, Support vector machine, Wavelet scattering network.

1. Introduction

The analysis of blood cells serves as a crucial diagnostic tool, providing insights into human health conditions and has been a focus of research for several decades. The intricate process of blood cell development, marked by gradual transformations from early stem cells, underscores the complexity of physiological processes within the human body. Traditionally, the classification of these transformations into healthy and malign types, or their constituent components, requires the expertise of highly trained haematologists. Traditional methodologies, heavily reliant on manual labour and expertise, often struggle to provide timely and accurate diagnoses. The complexities of blood cell development and the need for precise classification pose significant hurdles for haematologists. Additionally, the demand for enhanced diagnostic accuracy, streamlined laboratory processes, and the potential for expedited healthcare decision-making has prompted the exploration of advanced automated solutions.

The integration of artificial intelligence (AI) technology has brought about significant changes in the healthcare sector, particularly in improving diagnostic precision and optimizing workflow efficiency. AI has introduced automated assistance in diagnostics, expanded clinical operations, and implemented quantifiable imaging techniques.

In response to the need for early identification and precise diagnosis of illnesses, and to address the challenges related to the intricate analysis of

leukocyte images, many approaches incorporating data science and computer vision are proposed in the literature. The algorithms are designed to receive leukocyte images as input which undergo a predefined mathematical operation, yielding an output that reflects the patient's health condition. The image acquisition approach, illumination, staining artefacts, class imbalance, dataset insufficiency, similar appearance of class images, and varying maturity levels of leukocyte cells throw many unsolved issues into the analysis of these images.

This study proposes a leukocyte discrimination approach based on an invariant scattering network (ISN) or wavelet scattering network (WSN) that is analogous to a deep CNN with fixed filter weights at extremely low model complexity and execution time.

The novel features of this approach include the incorporation of the stationary wavelet channel fusion filtered (SWCFF) algorithm for image enhancement and the utilization of the invariant scattering network (ISN) for robust feature extraction.

This proposed system goes beyond conventional methodologies in biomedical image processing and machine learning. Leveraging the SWCFF algorithm enhances leukocyte images, preserving key details crucial for accurate analysis. Simultaneously, the ISN facilitates advanced feature learning, contributing to improved discrimination of leukocytes. The main advantages of this approach include enhanced diagnostic accuracy, reduced reliance on extensive manual labor, and the potential for expedited healthcare decision-making.

Through rigorous evaluation on benchmark datasets (ALLIDB, C_NMC, BCCD, and LISC), the proposed approach demonstrates superior results, achieving significant improvements in binary classification accuracy and outstanding accuracy for specific cell types. Precision rates and false positive rates further underscore the robustness of the proposed model. In summary, this innovative system showcases advancements in image enhancement and feature extraction, leading to unparalleled results with significant advantages over existing methodologies.

This paper is organized into five sections. Section 2 contains a comprehensive literature review covering the current research. Section 3 details the materials and methods employed in the research paper. Section 4 reports the results from extensive MATLAB-based simulations. Finally, in section 5, the paper concludes by summarizing key findings, emphasizing the methodology's significance, and discussing potential future research directions.

2. Literature review

The current medical routine for disease diagnosis relies on standard laboratory test results that are carried out instantly. Some of the usual tests are a complete blood cell count (counting the number of erythrocytes, leukocytes, and thrombocytes) and a differential blood cell count (counting the number of types of leukocytes: eosinophils, basophils, neutrophils, lymphocytes, and monocytes). To understand why automation of the leukocyte differential count is needed, it’s important to know the traditional approach. A drop of blood (usually 10mm3) is stained with some dye and spread over a glass slide for observation under the microscope. Expert pathologists validate the cells and their count manually [1, 2].

The automatic hematology instruments or machines currently accessible recognize and count five types of leukocytes using direct current, laser technology, and different blood smear slide staining techniques [3, 4]. These analyzers are insensitive in identifying immature, blast, or abnormal cells [5]. Hence, frequently, analyzers flag the samples with cell populations, suggesting the demand for peripheral smear examinations by skilled personnel to identify the anomalous cells. Apart from these, hematology analyzers are also subjective to various clinical conditions, such as the analyzer’s optical and electronic adjustments, preanalytical storage circumstances, lab technician skills, and awareness about the capabilities of analyzers [6]. This led to the emergence of computer vision and image processing (IP)-based techniques for the detection and discrimination of leukocytes in peripheral microscopic blood smear images.

A texture feature classification approach was proposed using a discrete orthonormal S transform model [7]. The features extracted from this model were used to train random forest [8] classifiers on the acute lymphoblastic leukemia image database (ALLIDB) [9]. A hybrid model was built with a monogenic wavelet scattering network: a cascade network of wavelet filters with nonlinear modulus and low-pass averaging operators [10, 11]. A traditional ML-based segmentation and classification model with new color features was proposed by [12] trying to address the difficulty in segmenting the cytoplasm of the cells. Three datasets: the Raabin white blood cell dataset (RWBCD), leukocyte images for segmentation and classification (LISC), and the blood cell count dataset (BCCD) were used to validate the method. An intelligent classification approach using an Elman neural network was put forth [13] to classify healthy and unhealthy cells. The

network used various wavelet functions at different hidden layers to increase generalization and search space compared to a simple neural network. An effective classification approach was proposed using ResNeXt [14] and a convolutional neural network (CNN) [15] with squeeze and excitation modules. The method was validated on the C_NMC [16] online challenge dataset. A finer classification model was built using a residual neural network to mitigate the challenges of distinct feature extraction and the inefficiency of handling fine-grained cases of classification. This approach used 100,000 labelled cell images of 40 different types. Leukemia and its four types, classification was presented [17] using deep CNN along with 7 different transformations (rotation, width shift, height shift, vertical flip, horizontal flip, shearing, and zoom) applied to augment the small datasets like ALLIDB and the American Society of Hematology bank.

Several challenges do exist in the leukocyte images that can adversely affect classification performance: sample similarity between various classes, dataset imbalance, sample insufficiency, illumination, and acquisition arteifacts to mention a few. A few of these issues were addressed by Hua Chen [18], who identified the advantage of combining two CNN models: Dense net and resnet along with spatial and channel attention modules (SAM and CAM). SAM identifies pixels of importance, and CAM [19] extracts crucial features from SAM pixels. The combined effect of SCAM takes care of sample similarity. Data augmentation was also performed to address insufficiencies in the dataset. The generalizability of the model can be improved by mixing up different class images that share common background pixels. The limitation of this model was its inability to focus on a loss function that can affect the tradeoff between interclass and intraclass variations. The implementation was carried out on a complex NVIDIA Titan Xp 12-gigabyte GPU.

A transfer learning approach by Erdal Basaran [20] was implemented by extracting discriminative features from the CNN squeeze net. The features were identified by the local interpretable model agnostic explanation (LIME) algorithm. LIME was developed to visualize areas contributing to classification scores. The minimum redundancy maximum relevance (mRMR) feature selection mode, subsets highly differentiable features and aids in reducing the feature space. To classify leukocyte types in low-resolution and noisy images, Xufeng Yao proposed a transfer learning-based classification model known as two-DCNN (two-module weighted optimized deformable CNN) [21]. The CNN image net was used to train good-quality images, and then the weights were moved to the second module to train low-quality and low-resolution images. A combination of the Gabor filter operator and CNN kernels was proposed [22], in which extracted features were more feasible and classifiable as the model transformed CNN kernels into a recurrence area that helped features learn various frequencies and directions.

Drawbacks of state of the art techniques are as follows:

- **Manual blood smear examination [1, 2]:** The traditional approach of manually staining blood smears and validating cell counts under a microscope is labor-intensive, time-consuming, and highly dependent on the expertise of pathologists. It lacks scalability and introduces subjectivity in cell identification, impacting the efficiency of the diagnostic process.
- **Automatic hematology instruments [3, 4, 5]:** Current automatic hematology instruments, while recognizing and counting five types of leukocytes, exhibit insensitivity to immature, blast, or abnormal cells. This limitation necessitates additional peripheral smear examinations by skilled personnel to accurately identify anomalous cells. The instruments' dependency on specific staining techniques and susceptibility to clinical conditions introduces variability in results.
- **Texture feature classification with s transform model [7, 8]:** The texture feature classification approach utilizing a discrete orthonormal S transform model may face challenges in handling diverse leukocyte images. While features extracted from this model are used for training classifiers, the approach might lack adaptability to variations in image characteristics, limiting its ability to capture nuanced patterns effectively.
- **ML-based segmentation and classification [12]:** Traditional machine learning-based segmentation and classification models, even with new color features, may struggle with accurately segmenting the cytoplasm of cells. The difficulty in addressing this segmentation challenge can impact the overall accuracy of classification, particularly when dealing with datasets such as Raabin white blood cell dataset (RWBCD), leukocyte images for segmentation and classification (LISC), and the blood cell count dataset (BCCD).
- **Elman neural network [13]:** The Elman neural network proposed for classifying healthy and

unhealthy cells using various wavelet functions at different hidden layers may encounter challenges related to generalization. While attempting to increase generalization and search space compared to a simple neural network, the effectiveness of this approach may be influenced by the complexity of the network architecture.

These drawbacks highlight the need for advanced techniques in leukocyte image analysis to overcome limitations associated with conventional methods.

In contrast to conventional methods such as manual blood smear examination and automatic hematology instruments, the proposed approach seeks to revolutionize leukocyte image analysis by addressing inherent limitations in accuracy, efficiency, and adaptability. While manual examination is labor-intensive and subjective, the proposed method leverages advanced computer algorithms, data science, and computer vision to automate the process, significantly reducing reliance on human intervention. Unlike automatic hematology instruments that may lack sensitivity to specific leukocyte types, the proposed model introduces a novel perspective by integrating the stationary wavelet channel fusion filtered algorithm and the Invariant scattering network. This innovative combination not only enhances image quality through the application of mathematical operations but also employs feature learning practices to analyze leukocyte pictures systematically. By doing so, the proposed model aims to overcome the challenges faced by traditional approaches and offers a more robust, precise, and scalable solution for the early diagnosis and detection of leukemia and other blood-related conditions. The emphasis on automatically extracted features and the integration of advanced algorithms positions this research at the forefront of leveraging artificial intelligence for transformative advancements in medical diagnostics.

The model efficiently extracts distinguishable features from the enhanced image dataset and classifies them using the classifier support vector machine (SVM). The image dataset is preprocessed using the stationary wavelet channel fusion filtered (SWCFF) model that enhances the quality of images validated using the naturalness image quality evaluator (NIQE), a blind image quality measure [23].

3. Materials and methods

The proposed leukocyte image classification model shown in Fig. 1 is characterised by different phases like pre-processing, feature extraction, and classification. Four benchmark datasets: ALLIDB, BCCD, C-NMC, and LISC dataset [24, 25, 26, 27, 28], are used with approximately 2000 images that include both binary class and multi-class. Firstly, datasets are subjected to image enhancement using the SWCFF model. Various features are extracted from intensified images using ISN and are classified using the SVM model.

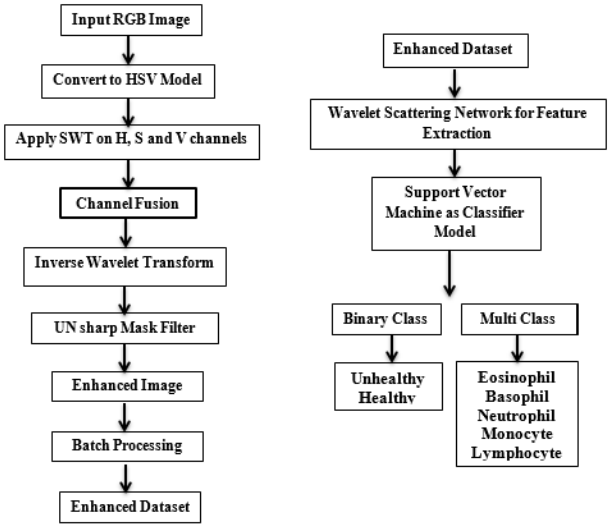

Figure. 1 Block diagram of leukocyte classification model

The images in the dataset are of low contrast and the region of interest (ROI) is not distinguishable from non-ROI. To address this issue, images are first preprocessed to enhance their quality. Image enhancement [29] has the power to improve image interpretability such that diagnostic features can be easily identified and extracted. The variant images from ALLIDB, BCCD, C-NMC, and LISC datasets are preprocessed: to minimize background noise, reduce illumination errors, sharpen edges, and contrast differences between foreground and background. Sample images from different datasets are shown in Fig. 2.

3.1 Preprocessing using SWCFF model

The red green blue (RGB) images are first resized to the standard size of 228×228 pixels and converted to hue saturation value (HSV), as it is more robust towards lighting variations. The HSV image is fragmented into its constituent channels. The stationary wavelet transform (SWT) is applied to extract approximate, vertical, horizontal, and diagonal coefficients from each channel. The H, S, and V SWT coefficients are fused [30] and inverse SWT is applied to the resultant fused coefficients. The average fusion rule is applied to approximate coefficients and the maximum fusion rule to detailed coefficients.

The fusion rules are as follows:

$$A = \frac{A1+A2+A3}{3} \quad (1)$$

$$H = \max(H4, H5) \; where \; H4 = max(H1, H2) \; and \; H5 = max(H2, H3) \quad (2)$$

$$V = max(V4, V5) \; where \; V4 = max(V1, V2) \; and \; V5 = max(V2, V3) \quad (3)$$

$$D = max(D4, D5) \; where \; D4 = max(D1, D2) \; and \; D5 = max(D2, D3) \quad (4)$$

In the above equations: A1, A2, and A3 are approximate; H1, H2, and H3 are horizontal; V1, V2, and V3 are vertical, and D1, D2, and D3 are diagonal coefficients of HSV channel images H, S and V respectively. The coefficients: A, H, V and D are obtained after applying fusion rules. These coefficients are combined using inverse SWT to get the resultant fused image. This image consists of crucial features of all three channel images. The fusion rules are applied according to the Eqs. (1) to (4) and composed back to generate a reconstructed image. Unsharp filtering is a technique of subtracting smoothed or unsharp version of an image from the original one. The original image is convolved with the standard discrete Laplacian filters. Mathematical equations on unsharp masking are shown below. Eq. (5) gives the mask and Eq. (6) the filtered image. The Laplacian filters can be any one of the 3 filters as shown in Eq. (7).

$$gmask(x, y) = f(x, y) - \bar{f}(x, y) \quad (5)$$

Where $f(x, y)$ is the original image, $\bar{f}(x, y)$ is the blur image.

$$g(x, y) = f(x, y) + k * gmask(x, y) \quad (6)$$

Unsharp filtered mask is $g(x, y)$ scaled with $k = 1$.

$$\begin{bmatrix} 0 & -1 & 0 \\ -1 & A+4 & -1 \\ 0 & -1 & 0 \end{bmatrix} \begin{bmatrix} -1 & -1 & -1 \\ -1 & A+8 & -1 \\ -1 & -1 & -1 \end{bmatrix} \begin{bmatrix} 1 & 1 & 1 \\ 1 & -8-A & 1 \\ 1 & 1 & 1 \end{bmatrix} \quad (7)$$

Three different masks can be used for filtering. The study used first mask.

The image enhancement steps are as follows:

- Resize input image to 228×228×3 pixels.
- Convert an RGB image to HSV color space.
- Separate the HSV image into 3 different channels H, S & V.
- Apply a 2-level SWT on each channel.
- Extract the approximate and detailed coefficients from each channel.
- Implement the fusion rules on the extracted coefficients.
- Reconstruct the original image using inverse SWT.
- filter the reconstructed SWT gray scale image using the unsharp mask
- calculate NIQE blind quality measure on the original and enhanced image for comparison.

The fused gray-scale image is passed through an unsharp mask filter to further enhance the leukocyte cells. Compute no reference quality measure using NIQE metric on original RGB input image and SWCFF enhanced images [31]. Compare and validate the enhancement. All pre-processing procedures were executed in MATLAB using the Image Processing Toolbox. The Fig. 3 depicts resultant sample images from all the four datasets respectively enhanced using SWCFF algorithm.

3.2 Feature extraction through ISN

The SWCFF-enhanced images are subjected to feature-extraction using ISN. MATLAB's Image Processing and Wavelet tool boxes were used to create the wavelet scattering framework [32]. The framework employs two banks of complex-valued 2-D Morlet filters (i.e., two scattering stages). The scattering disintegration outcome is determined by the parameters set in the framework. Invariance Scale (s), quality factors (q), and number of rotations (r) are among the parameters. The ISN chooses the time-invariant scale to be a discrete value using a specified number of wavelet filters. Selection of an appropriate unvarying scale would require a sound knowledge of dynamical shifts in the image under reference. The scattering framework is translation-invariant only up to the invariance scale. By default, MATLAB employs a quality factor of 8 in the first filter bank and a factor of 1 in the second. For image data, large quality factors are not needed. The same setting is retained in this work. A test was carried out to examine the extent to which alterations in certain parameter values affect the sensitivity of scattering properties. The test provided information on the

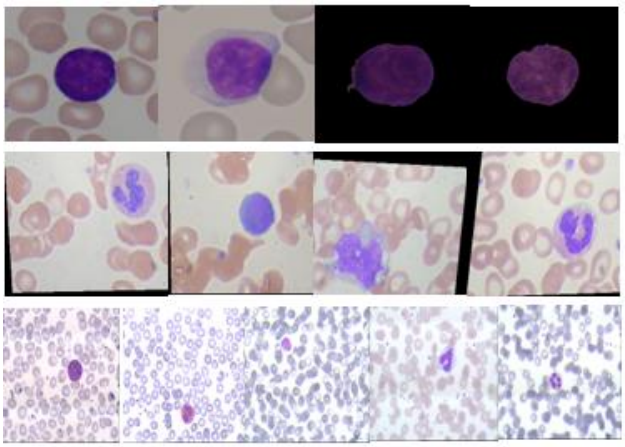

Figure. 2 Samples from dataset – Row 1: ALLIDB (All, healthy), C-NMC (All, healthy), Row2: BCCD (Eosinophil, Lymphocyte, Monocyte, and Neutrophil), Row3: LISC (Basophil, Eosinophil, Lymphocyte, Monocyte, and Neutrophil)

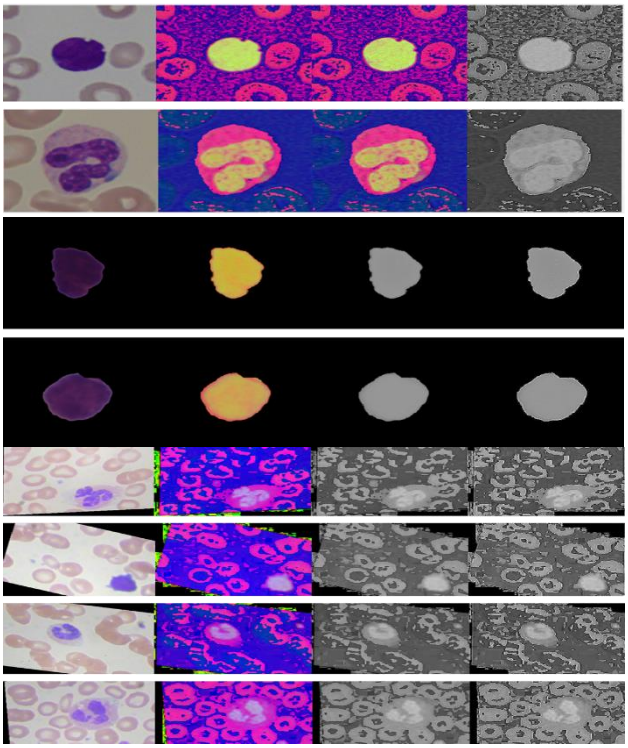

Figure. 3 SWCFF Enhanced image of all datasets (From left original raw image to right filtered image) (Images obtained from methodology results)

implication of differences in the means of a specific feature as a specified parameter is altered. When the scale invariance and quality factor parameters were modified, there was a substantial difference in the means for the majority of the attributes. However, not one of the features shows a statistically noteworthy variation in means when the amount of rotation parameter is changed. In the earlier iterations of the scattering framework, the parameters that were altered were limited to s and q. The q factor regulates the numeral of wavelets per interval (octave) in each of the filter banks. Although permitting wavelets within each octave may be advantageous because it allows for nuanced scale examination, it may also increase the processing complication of the framework if large number of wavelets are employed. As a result, a compromise must be reached somewhere in the middle. A two-layer image scattering network with an invariance scale of 40-by-40 pixel was built. The first layer has two wavelets per octave and the second layer has single wavelet per octave and two wavelet rotations per layer are set up. In the framework, the default value assigned to the s parameter is 150. The s factor values were tested within the range of [25 150] with an incremental step of 25. This default value does not imply the ideal value for the parameter. 40 invariance-scales were opted as it gave good results for the chosen image dataset. The features obtained from the WSN are low-variance, shift-invariant representations, and stable against spatial deformations [33].

Some mathematical notations and equations in WSN are as follows: Wavelet convolution is represented by the father and the mother wavelets which have known weights obtained without iteration. The father wavelet is represented by ϕ and the mother wavelet by ψ. The input image is first averaged using WLPF and then scaled with a mother wavelet resulting in layer 0 scatterings. The basic building block of WSN is continuous wavelet transform (CWT) which measures the similarity of image pixels with wavelets of varying frequency and scale, at each point in time. The modulus of CWT is convolved with low pass i.e., temporal averaging. Overall operation is shown in Eq. (8) as I order scattering coefficients – $\lambda 1$:as the center frequency of I order wavelets [34]. The convolution is of the LPF with every individual row of CWT. The second order scattering proceeds by convolving the modulus of CWT with second order wavelets. The second CWT is computed directly on the modulus of the first CWT i.e., the second order wavelets take the entire first CWT as input and convolve with every individual row of second CWT. The second order coefficients are obtained by convolving modulus with WLPF as in Eq. (9) Higher orders proceed in the same manner, convolving wavelets with a modulus of a previous order, followed by modulus and low pass filtering. The nth order scattering coefficient is shown in Eq. (10).

Scattering (I order)

$$S_1(t_1\lambda_1) = \left|x * \psi_{\lambda_1}\right| * \phi \quad (8)$$

Scattering (I order)

$$S_2(t_1\lambda_1\lambda_2) = \left|\left|x * \psi_{\lambda_1}\right| * \psi_{\lambda_2}\right| * \phi \quad (9)$$

Scattering (nth order)

$$S_n(t_1\lambda_1\lambda_n) = \left|\left|x * \psi_{\lambda_1}\right| * \dots\dots\dots\dots\dots\left|* \psi_{\lambda_n}\right| * \phi\right| \quad (10)$$

Wavelet scattering energy dilated wavelets:

$$\psi_\lambda(t) = 2^{\frac{-j}{Q}} * \psi\left(2^{\frac{-j}{Q(t)}}\right), with\ \lambda = 2^{\frac{-j}{Q}} \quad (11)$$

Wavelet Transform

$$w_x(t) = \{x * \phi(t),\quad x * \psi_\lambda(t)\} \quad (12)$$

If $\left|\hat{\phi}(w)\right|^2 + \sum_\lambda \left|\hat{\psi}_\lambda(w)\right|^2 = 1$ then w is unitary:

$$\|w_x\|^2 = \|x * \phi\|^2 + \sum_\lambda \|x * \psi_\lambda\|^2 = \|x\|^2 \quad (13)$$

Eqs. (11), (12), and (13) show that energy in the spatial domain is equal to the energy in the frequency domain [35].

To precis, the mother wavelets are decomposed to get father wavelets which are the actual features. The iterative utilization of the modulus of the wavelet transform facilitates the transfer of high-frequency energy from the original pixel to lower frequencies. At every step of transforming the energy in the lowest frequency band is obtained through convolution with ϕ. The remaining part is shifted towards the low frequency through a repeated application of the modulus of the wavelet transform and this process continues. The feature vectors are acutely down-sampled to minimize the mathematical complication of the network. The vectors that can be visualized and interpreted, are collectively called scattering features.

3.3 Classifier model design

The SVM classifier an exceptionally accepted classification model, is trained using train dataset with a cubic polynomial kernel and a one-verses-all coding scheme. The extracted features from ISN model are divided into train and test set in the ratio 80:20. The SVM hyperparameter selection process is speeded up with the employment of a technique for error-correcting output code with cross-validation of 5 to fit, and also automatically adjusts the SVM hyperparameters [36]. SVM is computationally efficient on small and large balanced dataset, require less memory space, and offer greater classification performance [37]. SVM is suitable for both small and large datasets as long as all its data points fall within the support vector hyper plane.

3.4 Assessment metrics

The trained SVM model is validated using a 20% test set for each enhanced image dataset. The model is assessed with various indicators like accuracy, specificity, recall (sensitivity), precision, false positive rate (FPR), f1-score, [38, 39], Cohen's kappa, etc. BCCD and LISC datasets are multi-class problems, hence per-class performances are calculated. The weighted mean between precision and recall is defined as the f1-score. Its value ranges between 0 and 1; from worst to best score.

For a binary classification problem, the confusion matrix is a 2×2 matrix with positive and negative values of target variables; while columns represent the actual values of target classes, the rows being the predicted values. True positive (TP) and true negative (TN) represent predicted value that exactly matches the actual value of the target class. The errors false positive (FP) and false negative (FN) are predicted classes that do not match with the actual class. False positives are of major concern in the medical field since infected cells will be misclassified as healthy cells. This prediction is a threat to humans if left untreated, due to incorrect detection eventually may lead to loss of life.

$$Accuracy = \frac{TP+TN}{TP+TN+FP+FN} \quad (14)$$

$$Precision = \frac{TP}{TP+FP} \quad (15)$$

$$Recall = \frac{TP}{TP+FN} \quad (16)$$

$$Specificity = \frac{TN}{TN+FP} \quad (17)$$

$$F1-Score = 2 \times \frac{Precision \times Recall}{Precision+Recall} \quad (18)$$

$$FPR = \frac{FP}{FP+TN} \quad (19)$$

Eqs. (14) to (19) depict the performance metrics. Since ALLIDB and NMC datasets are binary class is; but BCCD and LISC datasets are multi-class problems and hence these metrics cannot be directly

Table 1. Confusion matrix for two general class distributions

Actual Classification	Model's Prediction						
	K modes	p=1	…	p=h	…	p=k	Total
	a=1	n_{11}	…	n_{1h}	…	n_{1k}	n_{1T}
	…	…	…	…	…	…	…
	a=v	n_{v1}	…	n_{vh}	…	n_{vk}	n_{vT}
	…	…	…		…		
	a=k	n_{k1}	…	n_{kh}	…	n_{kk}	n_{kT}
	Total	n_{T1}	…	n_{Th}	…	n_{Tk}	N

applied to compute the performance. Instead, per-class performances are calculated [40, 41].

To investigate the concordance degree between model prediction and actual classification, in 1960 Cohen proposed a metric called Kappa Index 'K'. Cohen's Kappa index measures the correlation between predicted and actual class labels of any dataset [42]. It can be used to find the relation between the performances of different models having different cases.

The kappa index considers the actual class and predicted class as two independent variables. Marginal rows and marginal columns needed to compute K are extracted from the confusion matrix as shown in Table 1. and are given by Eq. (20). Eqs. (21) to (24) represent binary class Kappa index K computation formulae.

$$\frac{nvh}{nTh} = \frac{nvT}{N} \quad From\ this\ we\ can\ derive:$$

$$nvh = \frac{nTh\ .\ nvT}{N} \tag{20}$$

$$Binary\ class\ K = \frac{P_{ra} - P_{re}}{1 - P_{re}} \tag{21}$$

- Here, P_{ra} is the observed agreement or Model accuracy
- P_{re} is the expected agreement or expected accuracy.
- $1 - P_{re}$ is maximum value – minimum value of the Numerator.

Value is rescaled from -1 to $+1$.

$$P_{re} = P_{rpositive} + P_{rnegative} \tag{22}$$

$$P_{rpositive} = \frac{TP+FN}{N} . \frac{TP+FP}{N} \tag{23}$$

$$P_{rnegative} = \frac{TN+FP}{N} . \frac{TN+FN}{N} \tag{24}$$

Confidence interval (CI) [43] is a statistical measurement defined as, the probability that a parameter falls between certain ranges. It consists of like 95% or 99% of expected observations. For instance, if the observed accuracy of the machine learning model is 0.9615 then it's 95% CI is 0.9 to 1. This can be interpreted as; the model is 95% sure of its accuracy being in the range of 0.9 to 1 for a set of experiments. CI can be used to analyze well the statistical significance of certain predictions or estimations. If CI is zero, then it cannot be claimed that outcomes obtained from the results of experimentation are accreditable to a particular cause rather than it's by chance. The results of every phase of experiment are recorded and repeated for validation and confirmation. Eq. (25) gives the radius of the interval for CI with n being the sample size used for the test and Z representing the number of standard deviations from the Gaussian distribution. Z is technically termed binomial proportion CI. The Z values for various percentages of CI are 1.64 for 90%, 1.96 for 95%, 2.33 for 98% and 2.58 for 99%. Generally, 95% and 99% CI are used. The metric with a +/- radius of interval is calculated and displayed as CI.

$$Radius\ of\ Interval = Z \times \sqrt{\frac{metric*(1-metric)}{n}} \tag{25}$$

Interclass correlation coefficient (ICC) [44] is an inter-rater reliability measure used to find the reliability of ratings to the research data collected as groups from different people. Its value ranges from 0 to 1. A high value of ICC (close to 1) indicates high similarity among data from the same group and on the other side, low value indicates dissimilarity. One can measure ICC using Cohen's kappa as mentioned by Stephanie Glen [45]. Most of the researchers have evaluated their classifier models using equations 14 to 19. This study attempts to compute evaluation metrics like the kappa index and CI to validate the methodology.

4. Results and analysis

This work focuses on exploring how the ISN features obtained from SWCFF-enhanced images influence the classification performance. The experimentations involving binary and multiclass image datasets were performed on a PC with core i3-2350M CPU @2.3GHz, 8GB RAM, and windows 10 operating system. The simulation of the proposed methodology was performed using MATLAB 2019a. The first experiment was devoted to image

Table 2. Comparison of original and SWCFF enhanced images using NIQE metric

ALLIDB	Image files	Original Input Image (RGB)	Fused Image	Fused Filtered Image
ALL infected lymphoblasts	Im003_1__output	4.06	8.21	10.76
	Im001_1__output	4.16	7.38	10.88
	Im002_1__output	3.91	6.94	11.30
	Im122_1__output	4.13	6.78	15.11
Healthy lymphocytes	Im260_0__output	4.40	6.73	14.13
	Im132_0__output	4.06	10.69	12.22
	Im186_0__output	3.60	8.37	11.29
	Im227_0__output	3.92	8.66	14.21

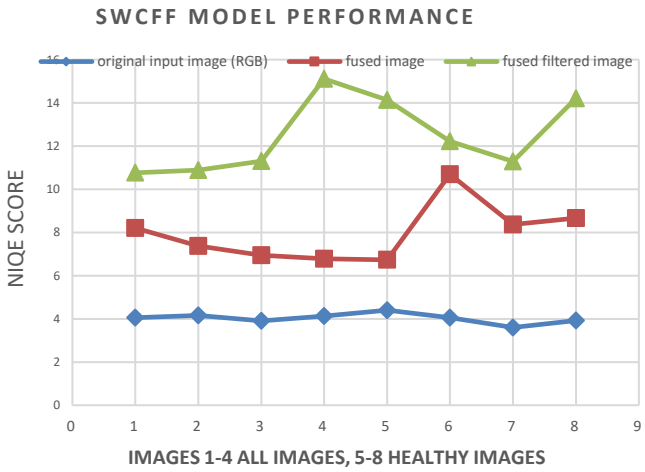

Figure. 4 SWCFF model performance for ALLIDB dataset

enhancement using the proposed SWCFF model. The images from all the datasets were processed, recorded, analyzed, and validated using NIQE blind image quality measure. The feature coefficients were extracted from: original RGB images; HSV converted images; wavelet decomposed fusion images; and finally, from fusion filtered images using ISN. The final experimentation was on the classification of enhanced images using SVM model. The pictures were divided into 80% training set and 20% test set. The confusion matrix was generated for fused filtered images of all the datasets. Table 2 provides NIQE scores computed at every step of the SWCFF algorithm for a few of sample images from ALLIDB. Images are named 'Imxxx_y_output', where x represents image number and y represents an unhealthy (1) lymphoblast cell or healthy (0) leukocyte cell. NIQE values clearly indicate that image quality has improved at each stage of the SWCFF model. The image fusion method proposed in this study has contributed in enhancing the original images as evident from the NIQE score depicted in Table 2 and in Fig. 4.

Table 3 shows a comparison of test accuracy, cross-validation accuracy, and loss for the datasets resulting from 5-fold cross-validation. Table 4 gives the conduct of the SVM classifier with metrics such as accuracy, precision, f1-score and recall (specificity) computed from the confusion matrix generated for the binary class: ALLIDB and NMC dataset. Since BCCD and LISC are 4 and 5-classed datasets respectively, their individual class metrics are calculated as shown in Tables 5 and 6. Tables 4, 5, and 6 also shows performance metrics computed for 95% CI. Figure 5 depicts the bar chart of actual and predicted class distribution. Fig. 6 displays performance metrics for all 4 datasets.

The results obtained from the experimentation using the SWCFF enhancement model and ISN feature extraction model and their influence on the performance of both binary and multiclass classification are presented in this section. It is evident from Table 3 that the SWCFF model results in pretty good accuracy for the ALLIDB dataset with 96.15% (95% CI of 0.9 to 1) and a minimum loss of 7.21%. It also depicts how accuracy improves step by step when images get transformed from original RGB to fusion-filtered images. The study investigates the inherent quality of wavelet features being consistent with local deformations, the scattering decomposition can capture vital discriminative features from images that are hard to detect amidst

Table 3. Comparison of test accuracy, cross validation accuracy and loss for all 4 datasets (in %)

Methodology	Dataset	Test Accuracy	Cross validation Accuracy	Loss
RGB	ALLIDB	76.92	75.96	24.03
	BCCD	33.33	30.07	69.92
	LISC	71.42	65.28	34.71
	C_NMC	69.23	65.38	34.61
HSV	ALLIDB	79.12	78.32	24.80
	BCCD	27.08	31.77	68.23
	LISC	65.30	67.35	32.64
	C_NMC	59.61	58.17	41.82
Fusion	ALLIDB	84.61	91.34	8.65
	BCCD	32.29	30.72	69.27
	LISC	65.30	65.28	34.71
	C_NMC	63.46	60.09	39.90
Fused filtered	ALLIDB	96.15	90.86	7.21
	BCCD	37.50	30.72	69.27
	LISC	75.51	67.87	32.12
	C_NMC	65.38	58.41	41.58

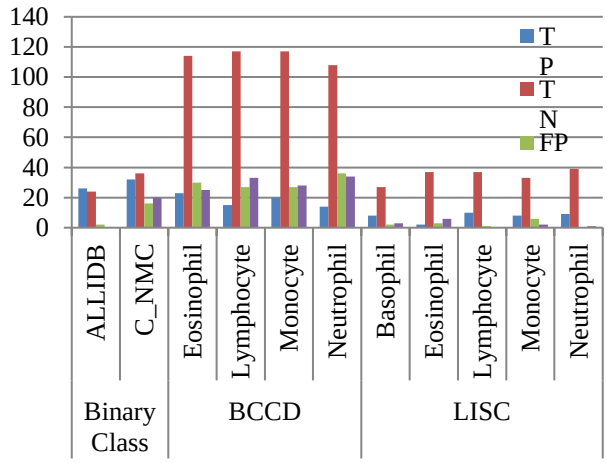

Figure. 5 Actual and predicted class distribution

Table 4. Binary class dataset performance measures (in %) with 95% CI (min value to max value)

DATASET	ALLIDB	C_NMC
Accuracy	96.15 (0.9 to1.00)	65.38 (0.53 to.78)
Precision	92.86 (0.85 to 0.99)	66.67 (0.54 to 0.79)
Recall	100	61.54 (0.48 to 0.75)
Specificity	92.31 (0.85 to 1)	69.23 (0.57 to 0.82)
F1-Score	96.30 (0.91 to 1)	64 (0.51 to0.77)
FPR	7.69 (0.5 to 0.07)	30.77 (0.43 to 0.13)
Kappa	92.30 (0.85 to 1)	30.76 (0.18 to 0.43)

illumination and staining artifacts but reflect the diagnostic condition of disease. Therefore, ISN is used to generate robust representations of leukocyte images that minimize variations within one leukocyte class while still retaining much-needed distinguishability between its types. Though ISN with filters not learned but are fixed well in advance and features are extracted not only from the last layers but are a combination of all the layers. It is evident that scattering coefficient energy reduces rapidly as layers increase, 99% of energy is present in the first two layers. Hence this study used only two layered scattering networks to extract the features. This reduces greatly the computational complexity and execution time (mean time for all datasets is 45 seconds). The classification accuracy is quite equally acceptable w.r.to ALLIDB and LISC Datasets with an accuracy of 96.15% (95% CI 0.9 to 1) and 89.66% (95% CI 0.72 to 1) (average) respectively. Thus, ISN is operational with minimal resources, less execution time, and with feature interpretability, it can be replaced with CNN under a moderately sized dataset environment. As can be seen from Table 4, the model could not perform well on C_NMC dataset since the cells in these images lacked texture details which resulted in the loss of valuable information that deteriorated when further processed. This can be addressed by more complex texture enhancement models.

Table 4 shows the performance of the multiclass BCCD dataset whose average class accuracy is 68.75% (95% CI 0.56to 0.82) and a minimum FPR of 0.19. These dataset images are characterized by similar sample appearance among classes and were easily misclassified. The monocytes and lymphocytes have a similar cell nucleus and poor background discrimination.

Table 6 depicts LISC dataset performance with the highest accuracy of 97.96%, precision and specificity maximum of 1, and ideal FPR of 0 for

Table 5. BCCD dataset performance measures (in %) with 95% CI (min value - max value)

BCCD	Eosinophil	Lymphocyte	Monocyte	Neutrophil	Average
Accuracy	71.35 (0.59 - 0.84)	68.75 (0.56 - 0.82)	71.35 (0.59 - 0.84)	63.54 (0.5 - 0.77)	69.01 (0.56 - 0.82)
Precision	43.41 (0.29 - 0.57)	35.71 (0.22 - 0 .49)	42.55 (0.29 - 0.57)	28.23 (0.15 - 0.41)	37.13 (0.24 - 0.51)
Recall	47.92 (0.34 - 0.62)	31.25 (0.18 - 0.44)	41.67 (0.28 - 0.56)	29.17 (0.16 -0.42)	38.12 (0.24 to0.51)
Specificity	79.17 (0.68 - 0.91)	81.25 (0.70 - 0.92)	81.25 (0.70 - 0.92)	75.12 (0.63 - 0.87)	79.02 (0.68 to 0.9)
F1-Score	45.54 (0.31 - 0.60)	33.33 (0.20 - 0.47)	42.11 (0.28 - 0.56)	28.57 (0.16 - 0.41)	37.23 (0.24 to 0.51)
FPR	20.83 (0.09 - 0.32)	18.75 (0.08 - 0.30)	18.75 (0.08 - 0.30)	25.0 (0.13 - 0.37)	21.0 (0.09 to 0.32)
Kappa	16.67 (0.16 - 0.17)				

Table 6. LISC dataset performance measures (in %) with 95% CI (min value - max value)

LISC	Basophil	Eosinophil	Lymphocyte	Monocyte	Neutrophil	Average
Accuracy	87.50 (0.67 - 1)	81.25 (0.54 - 1)	97.92 (0.89 - 1)	83.67 (0.60 - 1)	97.96 (0.89 - 1)	89.66 (0.72 - 1)
Precision	80.00 (0.56 - 1)	40.00 (0.06 - 0.74)	90.91 (0.73 - 1)	57.14 (0.26 - 0.88)	100	79.00 (0.63 - 0.94)
Recall	72.73 (0.46 - 0.99)	25.00 (-0.05 - 0.55)	100	80.00 (0.56 - 1)	90.00 (0.71 - 1)	85.00 (0.63 - 1)
Specificity	93.10 (0.78 -1.08)	92.50 (0.74 - 1.11)	97.37 (0.87 -1.07)	84.62 (0.62 -1.07)	100	92.00 (0.81 -1.03)
F1-Score	76.19 (0.51 - 1.01)	30.77 (-0.01 - 0.63)	95.24 (0.82 - 1.08)	66.67 (0.37- 0.96)	94.74 (0.81 - 1.09)	81.00 (0.59 - 1.02)
FPR	6.90 (-0.08 -0.22)	7.5 (-0.11 -0.26)	2.63 (-0.07 -0.13)	15.38 (-0.07 -0.38)	0.00	6.48 (-0.03 -0.19)
Kappa	69.23 (0.68 to 0.7)					

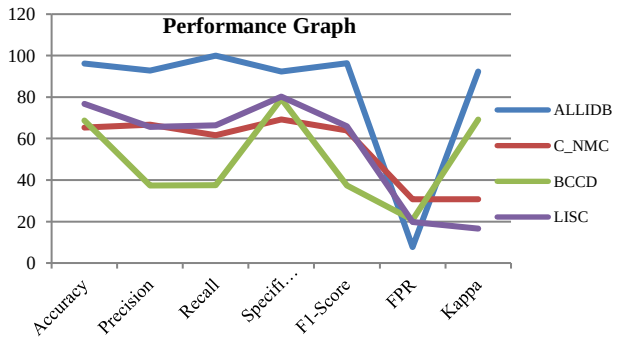

Figure. 6 Performance graph of binary and multi class dataset

neutrophil images. High specificity is evidence of reduced risk and no need to proceed with unnecessary painful biopsies in the later stages of the treatment. Similarly, high sensitivity or recall is a clear indication of accurate diagnosis i.e., presence or absence of disease. A kappa index of 92.30% for ALLIDB indicates model prediction is near perfect agreement with the actual class. Similarly, the kappa index of 69.23% for the LISC dataset presents model prediction is in a substantial agreement with the true class.

Table 7 (a) and b compares the proposed cell image classification system with state-of-the-art methods. In [17], Nizar Ahmed employs CNN on ALLIDB and ASH-Image bank, achieving accuracies of 88.25% and 81.74%, with high execution time on a single CPU and no image preprocessing. Sajad Tavakoli [12] addresses cytoplasm segmentation issues using LISC, achieving an accuracy of 92.21% and an F1 score of 94%, demonstrating robustness against staining artifacts. The accuracy of 96.15%, F1-Score of 96.30%, FPR of 7.69% for ALLIDB dataset and accuracy of 97.96%, F1-score of 94.74%, precision and specificity of 100% and least FPR of 0 for LISC dataset outperforms many CNN-based models as in Sajad Tavakoli (2021) and Hua Chen (2022) [46-54]. Hence, the SWCFF enhancement model and ISN have shown intense influence on classification performance.

Table 7 (a) Comparison of proposed system with existing state-of-the art methods (binary class dataset)

Study	Dataset Source	Techniques used	Performance Metric	Remarks
Nizar Ahmed (2019) [17]	ALLIDB	CNN	Accuracy- 88.25% 81.74%	High execution time since run on single CPU. No image preprocessing is done.
Proposed Model	ALLIDB	SWCFF+ISN+SVM	Accuracy-96.15% Recall-100% F1-score-96.3% FPR-7.69%	ISN analogous to CNN used without complex GPU H/W and tested on ALLIDB Dataset. Results match CNN models.

Table 7 (b) Comparison of proposed system with existing state-of-the art methods (multiclass dataset)

Study	Dataset Source	Techniques used	Performance Metric	Remarks
Sajad Tavakoli (2021) [12]	LISC	Segmentation (nucleus &cytoplasm) Feature Extraction (shape and color) SVM	Accuracy-92.21%, F1score-94%	Addressed issue in segmenting cytoplasm of cell. Robust and resilient against varying staining artefacts and imaging instruments
Hua Chen (2022) [18]	LISC, BCCD	Dense-Net & Resnet	Overall Accuracy 97.96%, 88.44%	Improved generalizability of the model by mix-up of images of different class that share common background pixels. Complex H/W needed
Proposed Model	LISC	SWCFF+ISN+ SVM	Accuracy-97.96% Precision-100%, Specificity-100% F1-Score-94.74%, FPR-0	ISN analogous to CNN used without complex GPU H/W and tested on LISC Dataset. Results match CNN models.

Hua Chen [18] uses dense-net and ResNet on LISC and BCCD, achieving overall accuracies of 97.96% and 88.44% respectively, with enhanced generalizability but requiring complex hardware. The proposed model, tested on ALLIDB and LISC datasets, achieves accuracies of 96.15% and 97.96%, respectively, excelling in specific metrics without the need for complex GPU hardware, using an ISN analogous to CNN [12, 17, 18].

The proposed new enhancement algorithm SWCFF gives comparable good results on ALLIDB, BCCD, C_NMC and LISC dataset. To best of our knowledge, we could hardly find any work in the literature that has implemented ISN on leukocyte blood cell images. This shows that this study is the first to use wavelet scattering features on leukocyte classification problem. The proposed methodology is highly reliable and robust for a balanced and unbalanced dataset of medical images without the need for complex hardware.

5. Conclusion

This study demonstrates a simulation of leukocyte classification problem using image-processing and machine-learning techniques on four benchmark datasets of peripheral blood smear images. The SWCFF channel fusion approach in preprocessing retains the key details of the image and aids the feature extraction process. The ISN; a minimal configuration network with low variance and insensitive to translations used to learn features is new and simple to implement. The binary classification accuracy has achieved a maximum of 96.15% and multi-class average accuracy of 90% on the benchmark dataset ALLIDB and LISC. The scattering network parameter settings and the type of 2-D channel image have a significant impact on detection accuracy. This study has evaluated the proposed model using an extensive metric set including statistics of point estimates; inter-subject correlations and confidence intervals. A contrast of the categorizing results got from this study with those acquired from a CNN highlights the potential of the suggested technology for leukocyte identification. The proposed methodology, when employed as a CAD tool, is very economical and can be deployed in remote areas or villages for early prediction of disease and timely monitoring of treatment. In the future, we will make an effort to investigate and enhance the system performance for BCCD and

C_NMC datasets and work on the conception of a highly durable system that can perform well on real-time cell images. Also, investigate detection-based systems and semantic segmentation-based classification models without using complex hardware.

Conflicts of interest

The authors declare no conflict of interest.

Author contributions

Renuka Veerappa Tali is the principal author responsible for the study's conception and design, overseeing experimental procedures, conducting data analysis, and composing the manuscript. She adeptly executed data acquisition and analysis, generated graphical representations. Surekha Borra served as the project supervisor, made substantial contributions to manuscript assessment and quality development. She was actively engaged in validity of study design, offering invaluable insights during data interpretation, and precisely revising the manuscript.

Acknowledgments

The present study did not get any dedicated financial support from public, commercial, or not-for-profit funding bodies.

References

[1] S. Acharjee, S. Chakrabartty, M. I. Alam, N. Dey, V. Santhi, and A. S. Ashour, "A semiautomated approach using GUI for the detection of red blood cells", In: *Proc. of International Conference on Electrical, Electronics, and Optimization Techniques (ICEEOT)*, pp. 525-529, 2016.

[2] V. Rajinikanth, N. Dey, E. Kavallieratou, and H. Lin, "Firefly algorithm-based Kapur's thresholding and Hough transform to extract leukocyte section from hematological images", In: *Proc. of Applications of Firefly Algorithm and its Variants*, Springer, Singapore, pp. 221-235, 2020.

[3] A. K. Fielding, S. Ager, and S. J. Russell, "ABC of clinical haematology: The future of haematology, molecular biology, and gene therapy", *BMJ*, Vol. 314, No. 7091, p. 1396, 1997.

[4] G. Chhabra, "Automated hematology analyzers: Recent trends and applications", *Journal of Laboratory Physicians*, Vol. 10, No. 1, pp. 015-016, 2018.

[5] G. Chhabra, "Automated hematology analyzers: Recent trends and applications", *J. Lab Physicians*, Vol. 10, No. 1, pp. 15-16, 2018, doi: 10.4103/JLP.JLP_124_17.

[6] J. J. Hoffmann and E. Urrechaga, "Recent advances in laboratory hematology reflected by a decade of CCLM publications", *Clinical Chemistry and Laboratory Medicine (CCLM)*, Vol. 61, No. 5, pp. 829-840, 2023.

[7] S. Mishra, B. Majhi, and P. K. Sa, "Texture feature-based classification on microscopic blood smear for acute lymphoblastic leukemia detection", *Biomedical Signal Processing and Control*, Vol. 47, pp. 303-311, 2019.

[8] P. J. Chun, I. Ujike, K. Mishima, M. Kusumoto, and S. Okazaki, "Random forest-based evaluation technique for internal damage in reinforced concrete featuring multiple nondestructive testing results", *Construction and Building Materials*, Vol. 253, No. 119238, 2020.

[9] A. Abhishek, R. K. Jha, R. Sinha, and K. Jha, "Automated classification of acute leukemia on a heterogeneous dataset using machine learning and deep learning techniques", *Biomedical Signal Processing and Control*, Vol. 72, No. 103341, 2022.

[10] W. H. Chak and N. Saito, "Monogenic wavelet scattering network for texture image classification", *JSIAM Letters*, Vol. 15, pp. 21-24, 2023.

[11] A. I. Sharaf, "Sleep Apnea Detection Using Wavelet Scattering Transformation and Random Forest Classifier", *Entropy*, Vol. 25, No. 3, p. 399, 2023.

[12] S. Tavakoli, A. Ghaffari, Z. M. Kouzehkanan, and R. Hosseini, "New segmentation and feature extraction algorithm for classification of white blood cells in peripheral smear images", *Scientific Reports*, Vol. 11, No. 1, pp. 19428, 2021.

[13] E. A. Boldbaatar, L. Y. Lin, and C. M. Lin, "Breast tumor classification using fast convergence recurrent wavelet Elman neural networks", *Neural Processing Letters*, Vol. 50, pp. 2037-2052, 2019.

[14] J. Prellberg and O. Kramer, "Acute lymphoblastic leukemia classification from microscopic images using convolutional neural networks", In: *Proc. of C-NMC Challenge: Classification in Cancer Cell Imaging: Select Proceedings, Springer Singapore*, pp. 53-61, 2019.

[15] G. Satyanarayana, P. A. Naidu, V. S. Desanamukula, and B. C. Rao, "A mass

correlation based deep learning approach using deep Convolutional neural network to classify the brain tumor", *Biomedical Signal Processing and Control*, Vol. 81, p. 104395, 2023.

[16] R. Gupta, S. Gehlot, and A. Gupta, "C-NMC: B-lineage acute lymphoblastic leukemia: A blood cancer dataset", *Medical Engineering & Physics*, Vol. 103, p. 103793, 2022.

[17] N. Ahmed, A. Yigit, Z. Isik and A. Alpkocak, "Identification of leukemia subtypes from microscopic images using convolutional neural network", *Diagnostics*, Vol. 9, No. 3, p. 104, 2019.

[18] H. Chen, J. Liu, C. Hua, J. Feng, B. Pang, D. Cao, and C. Li, "Accurate classification of white blood cells by coupling pre-trained ResNet and DenseNet with SCAM mechanism", *BMC Bioinformatics*, Vol. 23, No. 1, pp. 1-20, 2022.

[19] K. Wu and Y. Mei, "Multi-focus image fusion based on unsupervised learning", *Machine Vision and Applications*, Vol. 33, No. 5, p. 75, 2022.

[20] E. Basaran, "Classification of white blood cells with SVM by selecting SqueezeNet and LIME properties by mRMR method", *Signal, Image and Video Processing*, Vol. 16, No. 7, pp. 1821-1829, 2022.

[21] X. Yao, K. Sun, X. Bu, C. Zhao, and Y. Jin, "Classification of white blood cells using weighted optimized deformable convolutional neural networks", *Artificial Cells, Nanomedicine, and Biotechnology*, Vol. 49, No. 1, pp. 147-155, 2021.

[22] S. M. Raj, V. H. Deep, D. Chaudhary, and V. P. Singh, "A Pioneering and Streamlined Pixel Based Approach of Hyperspectral Image Classification for White Blood Cell Using Convolution Neural Network", *Annals of the Romanian Society for Cell Biology*, pp. 260-269, 2021.

[23] M. Pedersen and J. Y. Hardeberg, "Full-reference image quality metrics: Classification and evaluation", *Foundations and Trends® in Computer Graphics and Vision*, Vol. 7, No. 1, pp. 1-80, 2012.

[24] R. D. Labati, V. Piuri, and F. Scotti, "All-IDB: The acute lymphoblastic leukemia image database for image processing", In: *Proc. of 18th IEEE International Conference on Image Processing*, pp. 2045-2048, 2011.

[25] A. Gupta, R. Duggal, S. Gehlot, R. Gupta, A. Mangal, L. Mangal, and D. Satpathy, "GCTI-SN: Geometry-Inspired Chemical and Tissue Invariant Stain Normalization of Microscopic Medical Images", *Medical Image Analysis*, Vol. 65, p. 101788, 2020.

[26] R. Duggal, A. Gupta, and R. Gupta, "Segmentation of overlapping/touching white blood cell nuclei using artificial neural networks", *CME Series on Hemato-Oncopathology, All India Institute of Medical Sciences (AIIMS)*, New Delhi, India, 2016.

[27] R. Duggal, A. Gupta, R. Gupta, and P. Mallick, "SD-layer: stain deconvolutional layer for CNNs in medical microscopic imaging", In: *Proc. of Medical Image Computing and Computer Assisted Intervention, MICCAI 2017: 20th International Conference, Quebec City, QC, Canada, Part III 20*, Springer International Publishing, pp. 435-443, 2017.

[28] S. H. Rezatofighi and H. S. Zadeh, "Automatic recognition of five types of white blood cells in peripheral blood", *Computerized Medical Imaging and Graphics*, Vol. 35, No. 4, pp. 333-343, 2011.

[29] X. Guo, and Q. Hu, "Low-light image enhancement via breaking down the darkness", *International Journal of Computer Vision*, Vol. 131, No. 1, pp. 48-66, 2023.

[30] K. Parmar, R. K. Kher, and F. N. Thakkar, "Analysis of CT and MRI image fusion using wavelet transforms", In: *Proc. of International Conference on Communication Systems and Network Technologies*, IEEE, pp. 124-127, 2012.

[31] T. V. Renuka, B Surekha, D. B. Vijay, "CLAHE Enhanced Hybrid Feature Descriptors for Classification of Acute Lymphoblastic Leukemia in Blood Smear Images", *International Journal of Biomedical Engineering and Technology*, 2023.

[32] H. A. Agboola, and J. E. Zaccheus, "Wavelet image scattering based glaucoma detection", *BMC Biomedical Engineering*, Vol. 5, No. 1, p. 1, 2023.

[33] A. K. Saydjari and D. P. Finkbeiner, "Equivariant wavelets: Fast rotation and translation invariant wavelet scattering transforms", *IEEE Transactions on Pattern Analysis and Machine Intelligence*, Vol. 45, No. 2, pp. 1716-1731, 2022.

[34] Z. Liu, G. Yao, Q. Zhang, J. Zhang, and X. Zeng, "Wavelet Scattering Transform for ECG Beat Classification", *Computational and Mathematical Methods in Medicine*, 2020.

[35] I. Waldspurger, "Exponential decay of scattering coefficients", In: *Proc. of International Conference on Sampling Theory and Applications (SampTA)*, pp. 143-146, 2017.

[36] T. V. Renuka, and B. Surekha, "Acute-lymphoblastic leukemia detection through deep transfer learning approach of neural network", In: *Proc. of First Doctoral Symposium on Natural Computing Research: DSNCR 2020*, pp. 163-170, 2021.

[37] R. V. Tali, S. Borra, and M. Mahmud, "Detection and classification of leukocytes in blood smear images: State of the art and challenges", *International Journal of Ambient Computing and Intelligence (IJACI)*, Vol. 12, No. 2, pp. 111-139, 2021.

[38] P. Viertel, and M. König, "Pattern recognition methodologies for pollen grain image classification: a survey", *Machine Vision and Applications*, Vol. 33, No. 1, p. 18, 2022.

[39] S. O. Manoj, K. R. Abirami, A. Victor, and M. Arya, "Automatic Detection and Categorization of Skin Lesions for Early Diagnosis of Skin Cancer Using YOLO-v3-DCNN Architecture", *Image Analysis & Stereology*, Vol. 42, No. 2, pp. 101-117, 2023.

[40] M. Grandini, E. Bagli, and G. Visani, "Metrics for multi-class classification: an overview", *arXiv preprint arXiv:2008.05756*, 2020.

[41] Apache Spark, Evaluation Metrics - RDD-based API, 2018. Available online at: https://spark.apache.org/docs/latest/mllib-evaluation-metrics.html

[42] M. L. McHugh, "Interrater reliability: the kappa statistic", *Biochemia Medica*, Vol. 22, No. 3, pp. 276-282, 2012.

[43] G. Hommel, B. Röhrig, and M. Blettner, "Confidence Interval or P-Value: Part 4 of a Series on Evaluation of Scientific Publications", *Deutsches Ärzteblatt International*, Vol. 106, No. 19, pp. 335-339, 2009.

[44] S. Glen, "Intraclass Correlation" From StatisticsHowTo.com: Elementary Statistics for the rest of us!", Online available at: https://www.statisticshowto.com/intraclass-correlation/ kappa metric

[45] T. K. Koo, and M. Y. Li, "A Guideline of Selecting and Reporting Intraclass Correlation Coefficients for Reliability Research", *Journal of Chiropractic Medicine*, Vol. 15, No. 2, pp. 155-163, 2016.

[46] H. Abed and A. S. Mohammed, "Proposing an Efficient CNN Model for Detection of Acute Lymphoblastic Leukemia (ALL) using Transfer Learning", *International Journal of Advance Computational Engineering and Networking*, Vol. 10, No. 8, pp. 53-56, 2022.

[47] Q. U. Ain, S. Akbar, S. A. Hassan, and Z. Naaqvi, "Diagnosis of Leukemia Disease through Deep Learning using Microscopic Images", In: *Proc. of 2nd International Conference on Digital Futures and Transformative Technologies (ICoDT2)*, IEEE, pp. 1-6, 2022.

[48] C. D. Ruberto, A. Loddo, and G. Puglisi, "Blob detection and deep learning for leukemic blood image analysis", *Applied Sciences*, Vol. 10, No. 3, p. 1176, 2020.

[49] M. E. Karar, B. Alotaibi, and M. Alotaibi, "Intelligent medical IoT-enabled automated microscopic image diagnosis of acute blood cancers", *Sensors*, Vol. 22, No. 6, p. 2348, 2022.

[50] S. Mishra, B. Majhi, and P. K. Sa, "Glrlm-based feature extraction for acute lymphoblastic leukemia (all) detection", In: *Proc. of Recent Findings in Intelligent Computing Techniques: Proceedings of the ICACNI-2017*, Springer Singapore, Vol. 2, pp. 399-407, 2018.

[51] Z. Moshavash, H. Danyali, and M. S. Helfroush, "An Automatic and Robust Decision Support System for Accurate Acute Leukemia Diagnosis from Blood Microscopic Images", *Journal of Digital Imaging*, Vol. 31, pp. 702-717, 2018.

[52] L. F. Rodrigues, J. H. Silva, P. H. C. C. Gondim, J. F. Mari, and R. P. M. G. Brasil, "Leukocytes classification in microscopy images for acute lymphoblastic leukemia identification", In: *Proc. of 12th Computer Vision Workshop*, pp. 68-73, 2016.

[53] A.T. Sahlol, F.H. Ismail, A. Abdeldaim, and A. E. Hassanien, "Elephant herd optimization with neural networks: a case study on acute lymphoblastic leukemia diagnosis", In: *Proc. of 12th International Conference on Computer Engineering and Systems (ICCES)*, IEEE, pp. 657-662, 2017.

[54] K. Sridhar, A. R. Yeruva, P. N. Renjith, A. Dixit, A. Jamshed, and R. Rastogi, "Enhanced Machine learning algorithms Lightweight Ensemble Classification of Normal versus Leukemic Cel", *Journal of Pharmaceutical Negative Results*, pp. 496-505, 2022.